Magnons and Phonons Optically Driven out of Local Equilibrium in a Magnetic Insulator

Kyongmo An, Kevin S. Olsson, Annie Weathers, Sean Sullivan, Xi Chen, Xiang Li, Luke G. Marshall, Xin Ma, Nikita Klimovich, Jianshi Zhou, Li Shi, and Xiaoqin Li

Phys. Rev. Lett. **117**, 107202 — Published 30 August 2016

DOI: 10.1103/PhysRevLett.117.107202

Magnons and Phonons Optically Driven Out of Local Equilibrium in a Magnetic Insulator

Kyongmo An[1], Kevin S. Olsson[1], Annie Weathers[2], Sean Sullivan[3], Xi Chen[3], Xiang Li[3], Luke G. Marshall[3*], Xin Ma[1], Nikita Klimovich[1], Jianshi Zhou[2,3], Li Shi[2,3,†], and Xiaoqin Li[1,3,†]

[1]*Department of Physics, Center for Complex Quantum Systems, The University of Texas at Austin, Austin, Texas 78712, USA*
[2]*Department of Mechanical Engineering, The University of Texas at Austin, Austin, Texas 78712, USA*
[3]*Materials Science and Engineering Program, Texas Materials Institute, The University of Texas at Austin, Austin, Texas 78712, USA*

The coupling and possible non-equilibrium between magnons and other energy carriers have been used to explain several recently discovered thermally driven spin transport and energy conversion phenomena. Here, we report experiments in which local non-equilibrium between magnons and phonons in a single crystalline bulk magnetic insulator, $Y_3Fe_5O_{12}$, has been created optically within a focused laser spot and probed directly via micro-Brillouin light scattering. Through analyzing the deviation of the magnon number density from the local equilibrium value, we obtain the diffusion length of thermal magnons. By explicitly establishing and observing local non-equilibrium between magnons and phonons, our studies represent an important step toward a quantitative understanding of various spin-heat coupling phenomena.

The emerging field of spin caloritronics has been stimulated by a number of recent discoveries, such as large magnon thermal conductivity [1,2], spin Seebeck effect (SSE) [3-10], spin Peltier effect [11,12], magneto-Seebeck effect [13], and thermal spin transfer torque (STT) [14,15]. These discoveries hold promise for new technologies based on thermally driven spin transport phenomenon. For example, thermal-STT improves upon current STT-based memory devices by reducing the threshold current for STT-induced magnetic switching [16]. In addition, the large magnon thermal conductivity observed in some cuprate crystals can find potential applications for thermal management [1]. Moreover, the spin Seebeck and spin Peltier effects are being explored for applications in novel thermoelectric energy conversion devices.

The coupling and non-equilibrium between different energy carriers, namely magnons, phonons, and electrons plays an important role in the current theories of spin caloritronic phenomena. For example, in the magnon-mediated transverse SSE model [4,17], it is speculated that the magnon population is out of local equilibrium with the phonon bath. However, such local non-equilibrium has not been directly observed [18]. Indeed, to drive and observe non-equilibrium between magnons and phonons, a temperature gradient must be established within a length scale smaller than the distance over which magnons relax toward complete thermodynamic equilibrium with the phonon bath. Experimental studies on creating and detecting local magnon-phonon non-equilibrium, and probing its associated fundamental length scale, can help to further advance the field of spin caloritronics.

In this letter, we demonstrate that magnons and phonons can be driven out of local equilibrium in a bulk crystal of the magnetic insulator $Y_3Fe_5O_{12}$ (yttrium iron garnet, or YIG) that is irradiated by a focused laser beam to obtain a temperature gradient on the order of $10^6\ \mathrm{K\,m^{-1}}$, two orders of magnitude larger than those achieved in previous experiments [18,19]. Using the Brillouin light scattering (BLS) technique, we are able to directly probe both the phonon temperature and magnon number density at the same location. Our measurements show that the magnon number density in the laser spot is apparently lower than the local equilibrium value. The fact that one can drive magnons and phonons out of local equilibrium by localized heating within a few microns suggests that the characteristic coupling length between thermal magnons and phonons is comparable to or longer than a few microns in YIG. The measured deviation in magnon number density from equilibrium also allows us to obtain a thermal magnon diffusion length of about 3 μm based on a diffusion model. These findings are essential for reaching a microscopic understanding of a host of spin caloritronic phenomena and exploring their potential device applications.

We measured the temperature dependent magnon and phonon spectra using the micro-BLS technique as shown in Fig. 1 [19-21]. A green laser with a wavelength of $\lambda = 532\ \mathrm{nm}$ and power of 8 mW was used as the probing laser in all BLS measurements. An additional red laser with $\lambda = 660\ \mathrm{nm}$ was used to create local heating in some of the measurements. The power of the heating laser was varied from 0 to 19.1 mW. The beam sizes for the probing and heating lasers were obtained by fitting the beam intensity with a Gaussian function and were found to have an effective radius of $w_\mathrm{g} = 0.8\ \mu\mathrm{m}$ and $w_\mathrm{r} = 1.3\ \mu\mathrm{m}$, respectively. The YIG sample was oriented with the [110] direction normal to the surface, and an external magnetic field of 49.5 mT was applied along the $[1\bar{1}0]$ in-plane direction of the sample in all measurements.

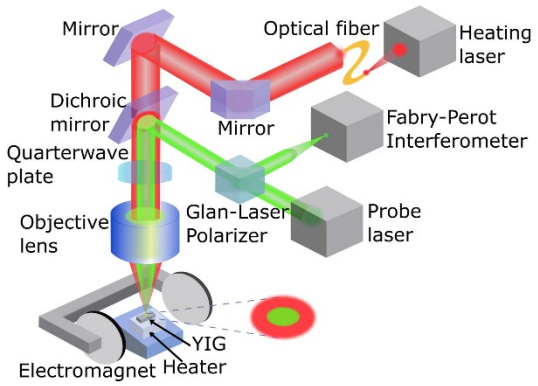

FIG. 1 Schematic of micro-BLS setup for measuring magnon and phonon BLS spectra in YIG under stage heating or focused laser heating.

We first discuss the magnon and phonon modes probed in the BLS spectra shown in Fig. 2. The dominant phonon and magnon modes probed by BLS have the same wave vector ($\boldsymbol{q}$) determined by the change in the photon momentum, as required by momentum conservation, $\boldsymbol{q} = \boldsymbol{k}_\mathrm{s} - \boldsymbol{k}_\mathrm{i}$, where $\boldsymbol{k}_\mathrm{s}$ and $\boldsymbol{k}_\mathrm{i}$ are the scattered and incident wave vectors of the laser averaged over the light cone, respectively. In our backscattering geometry, $\boldsymbol{k}_\mathrm{s}$ and $\boldsymbol{k}_\mathrm{i}$ are nearly anti-parallel, thus $\boldsymbol{q}$ equals $4\pi n/\lambda = 5.53 \times 10^7$ m^{-1}, where $n = 2.34$ is the index of refraction for YIG at $\lambda = 532$ nm [22]. This wave vector translates to a wavelength of 113 nm for both the magnon and phonon modes probed. The calculated frequencies of the probed magnon and phonon modes agrees well with our experimental observations (see the Supplemental Material [23] for details).

We first uniformly heated the YIG sample with an external heating stage while recording the temperature dependent BLS spectra, as shown in Fig. 2. While the phonon and magnon populations increase with temperature according to the Bose-Einstein distribution, the intensity, linewidth, and frequency of the BLS peak show complicated temperature dependence [45,46]. In Fig. 2a, the peak frequency in the magnon BLS spectra shifts downwards in frequency by 0.25 GHz when the temperature is increased from 302 K to 345 K. This shift arises from the reduction in the saturation magnetization with increasing temperature. As each magnon reduces the magnetic moment by the same amount, the measured magnon frequency shift can be used to probe the change in the local magnon number density. We note, however, that probing the magnon number density is insufficient to determine the magnon temperature when local non-equilibrium exists between magnons and the lattice within a length scale shorter than the magnon diffusion length. Within this length scale, a non-zero magnon chemical potential can produce an approximately constant magnon number density as the magnon temperature is changed [47,48].

The phonon BLS spectra exhibit a downward frequency shift of 0.14 GHz as the temperature increases

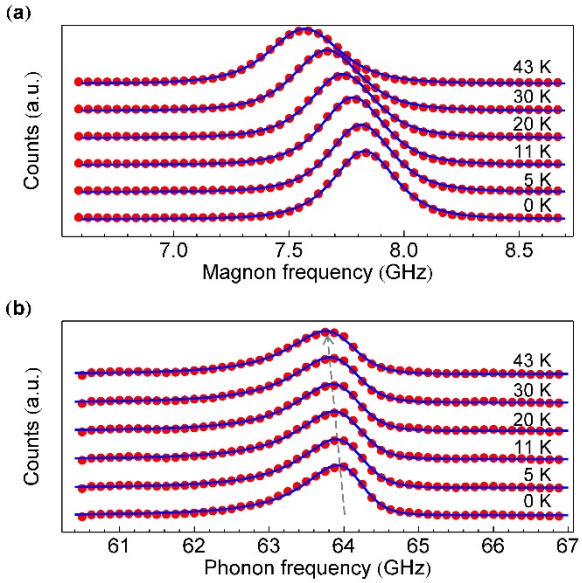

FIG. 2 Temperature dependent BLS spectra for (a) magnons and (b) phonons, obtained with the YIG sample heated uniformly on a heater stage. Solid lines are fitting using (a) symmetric and (b) asymmetric squared Lorentzian functions (see the Supplemental Material [23]). The arrow in (b) is drawn to show the small downward frequency shift of the phonon signal. The numbers inside the figure represent the stage temperature rise from the room temperature.

from 302 K to 345 K as shown in Fig. 2b. Because the phonon frequency shift is caused by bond softening and anharmonic coupling among phonon modes, the phonon frequency shift is influenced by the occupancy of all other phonon modes that are coupled to the long-wavelength phonon mode probed by BLS [45]. As such, the phonon peak shift can be used to probe the average temperature of the broad spectrum of thermally excited phonons instead of only the temperature corresponding to the long-wavelength mode directly probed by BLS.

In order to create and probe local non-equilibrium between magnons and phonons, we measured the phonon and magnon BLS spectra with the addition of a red heating laser while maintaining the sample stage at room temperature. Both the magnon and phonon frequencies shift down with increasing heating laser power (Fig. 3b) similar to the stage heating condition (Fig. 3a). Figure 3c shows the equivalent stage temperature rise for the stage heating condition that yields the same phonon frequency shift as that in the red laser heating experiment at each laser power. The difference in strain between the stage and laser heating cases were taken into account in Fig. 3c-d. (see the Supplemental Material [23] for detailed calculations of the strain effects and BLS measurements under hydrostatic pressure)

We now compare magnon frequency shifts in the two heating configurations. Figure 3d shows the magnon frequency shift as a function of the strain-corrected phonon frequency shift based on Fig. 3a and 3b. Because the measured phonon frequency shift is determined by

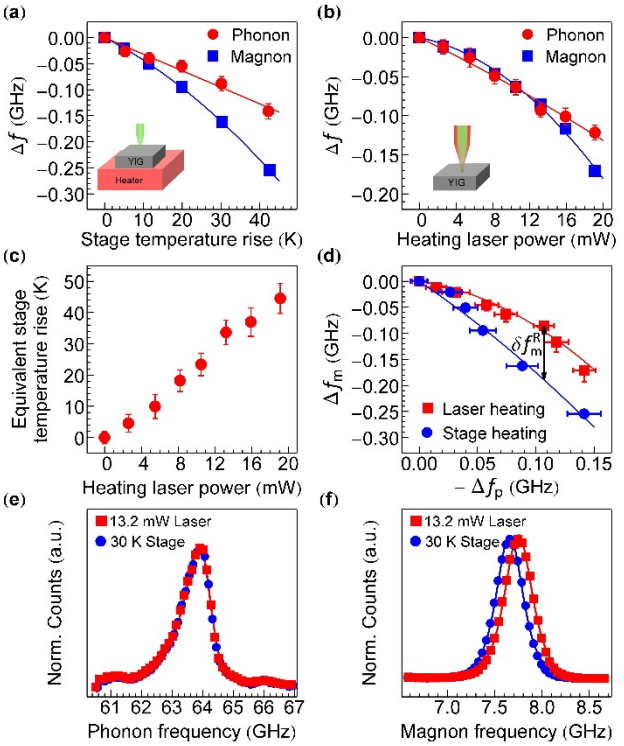

FIG. 3 (a) Peak frequency changes of magnons and phonons as a function of the sample stage temperature rise. The red line is a linear fitting of the phonon data while the blue line is a quadratic fitting of the magnon data. (b) Peak frequency changes for magnons and phonons as a function of the red heating laser power when the stage is kept at room temperature. The lines are polynomial fitting of the data. (c) Equivalent stage temperature rise in the stage heating measurement yielding the same strain-corrected phonon frequency downshifts in the laser heating measurement is plotted as a function of the heating laser power. (d) Magnon peak frequency changes (Δf_{m}) as a function of phonon peak frequency changes (Δf_{p}) in the two different heating configurations after the strain effects are accounted for. The arrow shows the difference $(\delta f_{\mathrm{m}}^{\mathrm{R}} > 0)$ in the magnon frequency between the 13.2 mW red laser heating and the corresponding stage heating that yields the same strain-corrected Δf_{p}. Raw BLS spectra of (e) phonon and (f) magnon under 30 K stage temperature rise (blue) and 13.2 mW laser heating (red). Solid lines are fitting. The spectra are normalized to their maximum counts.

the local phonon temperature rise when the strain effect is accounted for, the same x-axis value in Fig. 3d represents the same average local phonon temperature rise in the probe laser spot in two different heating experiments. It is apparent that the magnon frequency shift is smaller for the laser heating case than for the uniform stage heating condition. Specifically, we show two phonon/magnon spectra that have very similar averaged temperatures under stage heating (30 K) and laser heating (13.2 mW) in Fig. 3e and 3f. While the phonon spectral shapes are nearly identical (Fig. 3e), the magnon spectra are clearly shifted (Fig. 3f). As the magnon frequency shift is directly related to the magnon number density, this result clearly shows that the local magnon number density within the heating laser spot is not relaxed to the equilibrium value at the local phonon temperature. In comparison, two prior BLS measurements have been conducted in an attempt to directly verify the existence of local non-equilibrium in either magnetic insulators [18] or metals [19]. However, the ~10^4 K m^{-1} temperature gradients applied over mm scale were not sufficient to produce observable non-equilibrium between magnons and phonons.

To describe the established non-equilibrium between magnons and phonons quantitatively, we adopt the following steady state magnon diffusion equation, after using an averaged diffusion length l_{r} for the broad spectrum of thermal magnons [49],

$$\nabla^2 n = \frac{n - n_0}{{l_{\mathrm{r}}}^2}, \tag{1}$$

where n is the magnon number density, and n_0 is the magnon number density in local equilibrium with the phonon temperature $T_{\mathrm{p}}(\boldsymbol{r})$, which is calculated using the Bose-Einstein distribution $n_0 = \sum_{\boldsymbol{k}} \left[\exp\left(\frac{\hbar\omega(\boldsymbol{k})}{k_{\mathrm{B}} T_{\mathrm{p}}(\boldsymbol{r})}\right) - 1\right]^{-1}$, where $\hbar$ and k_{B} are the reduced Planck's constant and Boltzmann constant, respectively, $\hbar\omega(\boldsymbol{k})$ is the spectroscopic energy of the magnon mode with wave vector $\boldsymbol{k}$, and the summation is over all magnon modes. Each magnon decreases the magnetic moment by $g\mu_{\mathrm{B}}$, where g and μ_{B} are the Landé g-factor and the Bohr magneton, respectively. Therefore, the deviation from local equilibrium, $\delta n \equiv n - n_0$, leads to a deviation in the local magnetization, $\delta M = -g\mu_{\mathrm{B}}\delta n$. This deviation further gives rise to a deviation in the magnon peak frequency, $\delta f_{\mathrm{m}} \approx \left(\frac{\partial f_{\mathrm{m}}}{\partial M}\right)_{\mathrm{H}} \delta M = -\left(\frac{\partial f_{\mathrm{m}}}{\partial M}\right)_{\mathrm{H}} g\mu_{\mathrm{B}}\delta n$. Under the experimental conditions, we find that $\nabla^2 n_0 \approx \left(\frac{\partial n_0}{\partial T_{\mathrm{p}}}\right)_{\mathrm{H}} \nabla^2 T_{\mathrm{p}}$ is an accurate approximation [23]. Hence, Eq. (1) can be rewritten as

$$\nabla^2 T_{\mathrm{p}} + \nabla^2 \delta\theta_{\mathrm{m}} = \frac{\delta\theta_{\mathrm{m}}}{{l_{\mathrm{r}}}^2},$$

where

$$\delta\theta_{\mathrm{m}} \equiv \frac{\delta f_{\mathrm{m}}}{\left(\frac{\partial f_{\mathrm{m}}}{\partial T_{\mathrm{p}}}\right)_{\mathrm{H}}}. \tag{2}$$

Here, $\left(\frac{\partial f_{\mathrm{m}}}{\partial T_{\mathrm{p}}}\right)_{\mathrm{H}}$ depends on the local phonon temperature, $T_{\mathrm{p}}(r,z)$, and was obtained from the measurements of f_{m} at different stage temperatures with the heating from the green probe laser accounted for [23]. Equation (2) can be used to solve for $\delta\theta_{\mathrm{m}}(r,z)$, and subsequently $\delta f_{\mathrm{m}}(r,z)$.

The phonon temperature profile is determined by the steady state energy equation,

$$\nabla \cdot \left(\kappa_{\mathrm{p}} \nabla T_{\mathrm{p}}\right) + \nabla \cdot \left(\kappa_{\mathrm{m}} \nabla T_{\mathrm{m}}\right) + Q = 0\,, \qquad (3)$$

where κ_{m} and κ_{p} are the magnon and phonon contributions to the total thermal conductivity $\kappa = \kappa_{\mathrm{p}} + \kappa_{\mathrm{m}}$, and Q is the power density of the absorbed laser. Here, T_{m} is the magnon temperature. It has previously been found that κ_{m} is much smaller than κ_{p} in YIG near room temperature [50,51]. In addition, $\left|\nabla T_{\mathrm{p}}\right|$ is greater than $\left|\nabla\left(T_{\mathrm{p}} - T_{\mathrm{m}}\right)\right|$. Hence, the energy equation can be approximated as (see the Supplemental Material [23] for details of the energy equation),

$$\nabla \cdot \left(\kappa \nabla T_{\mathrm{p}}\right) + Q \approx 0\,. \qquad (4)$$

Eq. (2) and (4) were solved numerically using the commercial software COMSOL for both the red laser heating experiment at 13.2 mW and the stage heating condition with 33 K stage temperature rise, both of which yield the same strain-corrected phonon frequency shift in the probe laser spot according to Fig. 3c. The calculations were based on independently measured temperature-dependent thermal conductivity and absorption coefficients, and the green probe laser present in both heating configurations was taken into account explicitly. Figure 4a shows the difference in the local phonon temperature rise in the two simulations, $\Delta T_{\mathrm{p}}^{\mathrm{R}}(r,z)$, caused by the red heating laser. The weighted average value in the probe laser spot, $\langle \Delta T_{\mathrm{p}}^{\mathrm{R}}(r,z) \rangle$, is 32 K, which agrees with the equivalent stage temperature rise of 33 ± 4 K shown in Fig. 3c for the experiment at 13.2 mW heating laser power. The agreement verifies the phonon temperature measured by the BLS method. The corresponding magnon frequency deviation profile between the two heating conditions, $\delta f_{\mathrm{m}}^{\mathrm{R}}(r,z)$, is shown in Fig. 4b for $l_{\mathrm{r}} = 3.1\ \mu$m. The weighted average value $\langle \delta f_{\mathrm{m}}^{\mathrm{R}}(r,z) \rangle$ is plotted as a function of l_{r} in Fig. 4c. The black solid line and gray shaded area are shown to indicate the mean of the measured $\delta f_{\mathrm{m}}^{\mathrm{R}}$ and its uncertainty, respectively. From the intersection, we find $l_{\mathrm{r}} = 3.1 \pm 0.9\ \mu$m. The diffusion length obtained in our measurements corresponds to the value at about 372 K, due to the heating by both lasers. Because of the relatively long spin diffusion length compared to the heating laser spot size, the calculated magnon number density in the red laser heating experiment is lower than that in the stage heating condition, as shown in Fig. 4d, despite the same average phonon temperature in the probe laser spot. Details of the numerical calculations can be found in the Supplemental Material [23].

Our finding has important implications for spin caloritronics, where various relaxation processes of

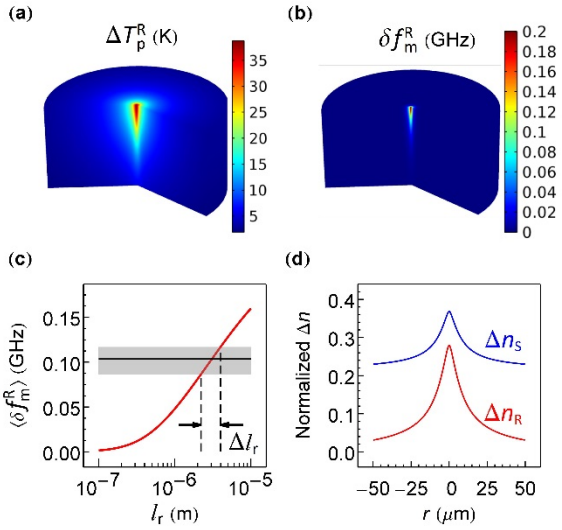

FIG. 4 Simulated spatial profiles of (a) the difference in the local phonon temperature rise in two simulations caused by the red laser heating and (b) magnon frequency deviation between the two heating conditions calculated with $l_{\mathrm{r}} = 3.1\ \mu$m. The displayed volume is 50 μm in both the radial and axial directions in both spatial profiles. (c) Weighted averages of $\delta f_{\mathrm{m}}^{\mathrm{R}}$ over the probe laser spot as a function of l_{r}. The red line shows the relation between each l_{r} used in the simulations and the calculated $\langle \delta f_{\mathrm{m}}^{\mathrm{R}} \rangle$. The gray area represents the uncertainty of measured $\delta f_{\mathrm{m}}^{\mathrm{R}}$ while the black solid line is the mean of measurements. Δl_{r} is the possible range of l_{r} for the calculated values due to the uncertainty of the measurement. (d) Simulated profiles of the magnon population rise relative to the room temperature value at the surface of YIG. The red and blue lines represent the magnon population rises for the red laser heating experiment (Δn_{R}) and the stage heating condition (Δn_{S}), respectively, as a function of position including the effect of the green probe laser. The magnon population rises are normalized by the room temperature value.

magnons play an important role. The scattering of magnons occurs by both spin-conserving and non-spin-conserving processes. Spin-conserving processes only relax energy and momentum. Such processes occur frequently and exhibit a length scale of a few nanometers according to thermal conductivity measurements [50]. On the other hand, non-spin-conserving processes relax the magnon number density through spin-orbit interactions with the lattice bath and may exhibit a longer length scale [52,53]. A long magnon spin diffusion length is considered essential for SSE [7,17]. While it has been suggested that this length could be as long as millimeters based on the initial SSE measurements [3,9], a recent measurement of magnon transport in a transverse SSE geometry has reported a magnon diffusion length of ~8 μm for thermally excited magnons in YIG near room temperature [54]. However, it has been suggested that the interpretation of transverse SSE measurements can be complicated by the presence of unwanted longitudinal thermal gradients in addition to

the intended transverse gradient in the experimental setup [55].

In summary, our experiments clearly demonstrate that magnons can be driven out of local equilibrium with the phonon bath in YIG when a large temperature gradient is generated on the scale of a few microns. Furthermore, our analysis shows that the observed local non-equilibrium is associated with a long thermal magnon spin diffusion length on the order of several microns. The optically-based non-contact method for exciting and probing non-equilibrium magnon transport demonstrated here can be extended to various materials where such properties remain unknown.

The authors thank David G. Cahill and Yaroslav Tserkovnyak for their insightful discussions on the strain effects and magnon diffusion theory, and acknowledge Jung-Fu Lin for valuable advice on the pressure cell design. KA, AW, XC, JZ, and LS were supported by the Army Research Office (ARO) MURI program under Award # W911NF-14-1-0016. Part of the support for KA and support for XM and XQL was provided as part of the SHINES, an Energy Frontier Research Center funded by the U.S. Department of Energy (DOE), Office of Science, Basic Energy Science (BES) under Award # DE-SC0012670. Work by KSO and SS was supported by National Science Foundation Thermal Transport Program under Award # CBET-1336968. AW is supported by an NSF Graduate Research Fellowship. The BLS instrumentation for the measurements under different heating was obtained via support from Airforce Office of Scientific Research (AFOSR) under grant # FA9550-08-1-0463 and FA9550-10-1-0022. The BLS instrument for the pressure-dependent measurement was obtained via support from ARO grant # W911NF-14-1-0536.

---

*Present address: Department of Chemical Engineering, Northeastern University, Boston, Massachusetts 02115, USA
†Authors to whom correspondence should be addressed. Email: elaineli@physics.utexas.edu, lishi@mail.utexas.edu

[1] C. Hess, B. Büchner, U. Ammerahl, L. Colonescu, F. Heidrich-Meisner, W. Brenig, and A. Revcolevschi, Phys. Rev. Lett. **90**, 197002 (2003).
[2] M. Hofmann, T. Lorenz, K. Berggold, M. Grüninger, A. Freimuth, G. S. Uhrig, and E. Brück, Phys. Rev. B **67**, 184502 (2003).
[3] K. Uchida, S. Takahashi, K. Harii, J. Ieda, W. Koshibae, K. Ando, S. Maekawa, and E. Saitoh, Nature **455**, 778 (2008).
[4] G. E. W. Bauer, E. Saitoh, and B. J. van Wees, Nature Mater. **11**, 391 (2012).
[5] M. Johnson, Solid State Commun. **150**, 543 (2010).
[6] S. R. Boona, R. C. Myers, and J. P. Heremans, Energy Environ. Sci. **7**, 885 (2014).
[7] J. Xiao, G. E. W. Bauer, K. Uchida, E. Saitoh, and S. Maekawa, Phys. Rev. B **81**, 214418 (2010).
[8] C. M. Jaworski, J. Yang, S. Mack, D. D. Awschalom, J. P. Heremans, and R. C. Myers, Nature Mater. **9**, 898 (2010).
[9] K. Uchida *et al.*, Nature Mater. **9**, 894 (2010).
[10] A. Kehlberger *et al.*, Phys. Rev. Lett. **115**, 096602 (2015).
[11] M. Hatami, G. E. W. Bauer, Q. Zhang, and P. J. Kelly, Phys. Rev. B **79**, 174426 (2009).
[12] J. Flipse, F. K. Dejene, D. Wagenaar, G. E. W. Bauer, J. B. Youssef, and B. J. van Wees, Phys. Rev. Lett. **113**, 027601 (2014).
[13] M. Walter *et al.*, Nature Mater. **10**, 742 (2011).
[14] H. Yu, S. Granville, D. P. Yu, and J. P. Ansermet, Phys. Rev. Lett. **104**, 146601 (2010).
[15] G.-M. Choi, C.-H. Moon, B.-C. Min, K.-J. Lee, and D. G. Cahill, Nature Phys. **11**, 576 (2015).
[16] J. C. Leutenantsmeyer *et al.*, SPIN **03**, 1350002 (2013).
[17] H. Adachi, K. Uchida, E. Saitoh, and S. Maekawa, Rep. Prog. Phys. **76**, 036501 (2013).
[18] M. Agrawal, V. I. Vasyuchka, A. A. Serga, A. D. Karenowska, G. A. Melkov, and B. Hillebrands, Phys. Rev. Lett. **111**, 107204 (2013).
[19] D. R. Birt, K. An, A. Weathers, L. Shi, M. Tsoi, and X. Li, Appl. Phys. Lett. **102**, 082401 (2013).
[20] S. O. Demokritov and V. E. Demidov, IEEE Trans. Magn. **44**, 6 (2008).
[21] B. Hillebrands, in *Light Scattering in Solids VII*, edited by M. Cardona, and G. Güntherodt (Springer, Berlin, 2000), pp. 174.
[22] G. B. Scott, D. E. Lacklison, and J. L. Page, Phys. Rev. B **10**, 971 (1974).
[23] See Supplemental Material [url], which includes Refs.[24-44]
[24] S. Kimura and I. Shindo, J. Cryst. Growth 41, 192 (1977).
[25] D. Rodic, M. Mitric, R. Tellgren, H. Rundlof, and A. Kremenovic, J. Magn. Magn. Mater. 191, 137 (1999).
[26] W. Hayes and R. London, *Scattering of Light by Crystals* (Wiley, New York, 1978).
[27] H. Suhl, J. Phys. Chem. Solids 1, 209 (1957).
[28] J. R. Sandercock and W. Wettling, Solid State Commun. 13, 1729 (1973).
[29] A. Aharoni, J. Appl. Phys. 83, 3432 (1998).
[30] W. Wettling, M. G. Cottam, and J. R. Sandercock, J. Phys. C: Solid State Phys. 8, 211 (1975).
[31] Y. A. Burenkov and S. P. Nikanorov, Phys. Solid State 44, 318 (2002).
[32] A. L. Stancik and E. B. Brauns, Vibrational Spectroscopy 47, 66 (2008).
[33] G. Rabilloud, *High-Performance Polymers: Chemistry and Applications* (Editions Technip, Paris, 1997).
[34] T. S. Narasimhamurty, *Photoelastic and Electrooptic Properties of Crystals* (Plenum Press, New York, 1981).
[35] R. W. Dixon, J. Appl. Phys. 38, 5149 (1967).
[36] D. E. Eastman, J. Appl. Phys. 37, 2312 (1966).
[37] S. Chikazumi, *Physics of Magnetism* (John Wiley & Sons, Inc., New York, 1964).
[38] R. L. Comstock, Proceedings of the IEEE 53, 1508 (1965).
[39] I. P. Kaminow and R. V. Jones, Phys. Rev. 123, 1122 (1961).
[40] D. Bloch, J. Phys. Chem. Solids 27, 881 (1966).

[41] G. T. Hohensee, R. B. Wilson, J. P. Feser, and D. G. Cahill, Phys. Rev. B 89, 024422 (2014).
[42] D. Sanders and D. Walton, Phys. Rev. B 15, 1489 (1977).
[43] B. Liao, J. Zhou, and G. Chen, Phys. Rev. Lett. 113, 025902 (2014).
[44] W. Cai, A. L. Moore, Y. Zhu, X. Li, S. Chen, L. Shi, and R. S. Ruoff, Nano Lett. 10, 1645 (2010)
[45] K. S. Olsson, N. Klimovich, K. An, S. Sullivan, A. Weathers, L. Shi, and X. Li, Appl. Phys. Lett. **106**, 051906 (2015).
[46] J. R. Sandercock, in *Light Scattering in Solids III*, edited by M. Cardona, and G. Guentherodt (Springer, Berlin, 1982).
[47] S. O. Demokritov, V. E. Demidov, O. Dzyapko, G. A. Melkov, A. A. Serga, B. Hillebrands, and A. N. Slavin, Nature **443**, 430 (2006).
[48] L. J. Cornelissen, K. J. H. Peters, G. E. W. Bauer, R. A. Duine, and B. J. van Wees, arXiv:1604.03706.
[49] G. Chen, *Nanoscale Energy Transport and Conversion: a Parallel Treatment of Electrons, Molecules, Phonons, and Photons* (Oxford University Press, New York, 2005).
[50] S. R. Boona and J. P. Heremans, Phys. Rev. B **90**, 064421 (2014).
[51] K. Uchida, T. Kikkawa, A. Miura, J. Shiomi, and E. Saitoh, Phys. Rev. X **4**, 041023 (2014).
[52] B. Flebus, S. A. Bender, Y. Tserkovnyak, and R. A. Duine, arXiv:1510.05316.
[53] D. Beeman and P. Pincus, Phys. Rev. **166**, 359 (1968).
[54] L. J. Cornelissen, J. Liu, R. A. Duine, J. B. Youssef, and B. J. van Wees, Nature Phys. **11**, 1022 (2015).
[55] S. Y. Huang, W. G. Wang, S. F. Lee, J. Kwo, and C. L. Chien, Phys. Rev. Lett. **107**, 216604 (2011).